Journal of Alloys and Compounds 707 (2017) 20–26

Contents lists available at ScienceDirect

Journal of Alloys and Compounds

journal homepage: http://www.elsevier.com/locate/jalcom

Phase transitions in Cu-based alloys under high pressure torsion

B.B. Straumal [a, b, c, *], A.R. Kilmametov [b], A. Korneva [d], A.A. Mazilkin [a, b], P.B. Straumal [c, e], P. Zięba [d], B. Baretzky [b]

[a] Institute of Solid State Physics, Russian Academy of Sciences, 142432, Chernogolovka, Russia
[b] Karlsruher Institut für Technologie, Institut für Nanotechnologie, 76344, Eggenstein-Leopoldshafen, Germany
[c] Laboratory of Hybrid Nanomaterials, National University of Science and Technology «MISIS», Leninskii Prosp. 4, 119049 Moscow, Russia
[d] Institute of Metallurgy and Materials Science, Polish Academy of Sciences, Reymonta St. 25, 30-059, Cracow, Poland
[e] A.A. Baikov Institute of Metallurgy and Materials Science, Russian Academy of Sciences, Leninskii Prosp. 49, 117991, Moscow, Russia

ARTICLE INFO

Article history:
Received 20 September 2016
Received in revised form
2 December 2016
Accepted 5 December 2016
Available online 7 December 2016

Keywords:
High-pressure torsion
Precipitation
Decomposition of solid solution
Phase transitions

ABSTRACT

Severe plastic deformation not only leads to grain refinement but also accelerates mass-transfer and drives phase transformations in these Cu-based alloys. This review is devoted to the dynamic equilibrium between decomposition of (supersaturated) solid solution and dissolution of precipitates during high pressure torsion (HPT) of diluted Cu-based Cu–X alloys. The precipitation of second phase particles from a solid solution and their dissolution take place simultaneously and compete with each other. During HPT, a certain steady-state concentration C_s of a second component in a solid solution is reached, as if a sample would be annealed at a certain effective temperature T_{eff}. We found that T_{eff} linearly increases with increase of activation enthalpy of bulk tracer diffusion H_D. The correlation between activation enthalpy of bulk tracer diffusion H_D and melting temperature T_m of diffusing alloying component has been found for the first time. As a result, T_{eff} linearly increases with increase of melting temperature T_m of diffusing alloying component as well. The observed correlations allow one for the first time to predict the behaviour and phase transitions in the Cu-based alloys under high pressure torsion.

1. Introduction

Severe plastic deformation (SPD) is a family of novel methods permitting metallurgists and engineers tailoring the structure and properties of materials [1]. The idea of SPD is to deform the material in a confined space. It allows an increase of the strain up to the enormous values without fracture. Since the material cannot break, the dynamic equilibrium between deformation-driven production of crystal defects and their relaxation (annihilation) is established after a certain strain value is reached. It is not astonishing that such a strong action on the material leads to various phase transformations [2,3] e.g. the formation [4,5] or decomposition [6–8] of a supersaturated solid solution, dissolution of phases [9–13], disordering of ordered phases [14,15], amorphization of crystalline phases [2,16–19], synthesis of the low-temperature [11,13], high-temperature [20] or high-pressure [21–23] allotropic modifications, and nanocrystallization in the amorphous matrix [24–27].

This review paper is devoted to the decomposition of (supersaturated) solid solution and the dissolution of precipitates during SPD. Recently it has become clear that they are not independent [28]. Moreover, the precipitation of particles of a second phase from a solid solution and their dissolution take place simultaneously and compete with each other. Due to the competition between precipitation and dissolution, a certain steady-state concentration of a second component in a solid solution is reached under SPD.

Quite frequently, this steady-state concentration of a second component in a solid solution after SPD is the same as it would appear in a material after long anneal at a certain (elevated) temperature. This temperature is called effective temperature T_{eff}. It has been demonstrated recently that the concept of effective temperature T_{eff} originally proposed for the materials under severe irradiation [28] is applicable also for severe plastic deformation (SPD) [29]. If the atomic movements driven by an external action (deformation or irradiation) are higher than those driven by the conventional thermal diffusion, the material is forced into a state which is equivalent to that at a certain increased (effective) temperature T_{eff}. One can estimate T_{eff} if the phases in a material after SPD treatment differ from those before SPD [30]. For the

* Corresponding author. Institute of Solid State Physics, Russian Academy of Sciences, 142432, Chernogolovka, Russia.
E-mail addresses: straumal@issp.ac.ru, straumal@mf.mpg.de (B.B. Straumal).

http://dx.doi.org/10.1016/j.jallcom.2016.12.057
0925-8388/

determination of T_{eff} one can use also the phase diagrams at high pressure, if they are known [21–23]. However, the SPD-treatment at ambient temperature T_{SPD} usually leads to the very quick phase transformations, which is easy to understand if one considers the high density of defects, similar to that at an increased temperature. The increased pressure, oppositely, leads to a decrease of diffusivity and/or grain boundary mobility [31,32]. Some SPD-driven phase transformations need only a small shift of atoms, for other ones long-range mass transfer is needed. The results of such SPD-driven transitions cannot be explained by the bulk or even grain boundary diffusion at the SPD temperature (which usually remains slightly above ambient one). Nevertheless, during the SPD-driven mass transfer an external action forces the atoms to overcome a certain energy barrier. This energy barrier is similar to that for bulk diffusion. The measure for this barrier is the activation enthalpy of bulk diffusion H_D. In this review the T_{eff} will be determined for various Cu-based alloys. Further, the correlation between T_{eff} and activation enthalpy of bulk diffusion H_D of an alloying component will be analyzed. It will be shown that H_D correlates with the melting temperature T_m of an alloying component in Cu-based alloys as well. In turn, T_{eff} also correlated with T_m. This allows on for the first time to predict T_{eff} knowing the T_m.

2. Determination of effective temperature

External action on the material can cause an accelerated mass transfer and phase transformations. Such accelerated diffusion and unusual phase transitions were first observed under severe irradiation of materials [29]. G. Martin was first who proposed a model to describe solid solutions subjected to irradiation-induced atomic mixing [29]. His main idea was that the forced mixing induced by irradiation corresponds to the increase of entropy. As a result, the severe irradiation changes the thermodynamic potentials in an alloy. In a simple case of regular solution in the Bragg-Williams approximation, a law of corresponding states was formulated: The equilibrium configuration of the solid under irradiation flux φ at temperature T is identical to the configuration at $\varphi = 0$ and a certain effective temperature.

$$T_{eff} = T(1 + \Delta) \quad (1)$$

One can describe the irradiation-driven movements of atoms by the "ballistic" diffusion coefficient D_{ball} if they are similar in amplitude to conventional diffusion jumps with conventional bulk diffusion coefficient D_b. In this case $\Delta = D_{ball}/D_b$. D_b can be increased due to the non-equilibrium defect concentration [23]. Thus, Martin proposed to use the equilibrium phase diagram for the description of the system under irradiation. However, the phases under irradiation are identical to those at T_{eff} instead of the temperature of experiment T. For example, the amorphous phase would appear under irradiation, if the liquid phase is present in the phase diagram at T_{eff} [29,33].

To check the applicability of Martin's law (1) to the forced diffusion driven by pure shear deformation under high pressure torsion (D_{HPT}) instead of irradiation (D_{ball}), we analyzed the experiments where HPT leads to the phase transitions. We compare the data obtained in similar straining conditions, namely those where (i) HPT was performed at 4–6 GPa with 4–6 torsions and (ii) the phases appeared after HPT are different from those present in the samples before HPT.

For the first time the HPT-driven decomposition of supersaturated solid solution was found in the Al–Zn alloys [6,7,34]. The (Al) solid solution in the as-cast Al–30 wt% Zn alloy contained about 15 wt% Zn. At room temperature (being also the HPT temperature) Zn is almost not soluble in solid Al. Therefore, the (Al) solid solution was strongly supersaturated. The as-cast Al–20 wt% Zn and Al–10 wt% Zn alloys contained, respectively, about 7 and 3 wt% Zn in the supersaturated solid solution. The HPT at room temperature produced nanograined pure Al and pure Zn particles simultaneously leading to unusual softening [6,7,34]. In all three alloys the supersaturated solid solution completely decomposed, and the lattice parameter became indistinguishable from that of pure aluminium. The respective $T_{eff} = 30$ °C. The decomposition during SPD proceeds extremely quickly, already after about 0.5 rotations of the anvils, the lattice parameter becomes equal to that of Al and microhardness as well as grain sizes reach their stationary values [34].

The homogenized one-phase solid solutions in the Cu–Ni alloys with 42 and 77 wt % Ni decomposed after HPT at room temperature into Cu-rich and Ni-rich phases [8]. The composition of resulting phases permitted an estimation of $T_{eff} = 200$ °C for the Cu–77 wt% Ni alloy and $T_{eff} = 270$ °C for the Cu–42 wt% Ni alloy [8]. In case of Co-rich Co–Cu alloys, the as-cast Co–12 wt% Cu alloy contained the supersaturated solid solution with 8 wt% Cu in the Co matrix with fcc α-structure [30]. After HPT, together with grain refinement, the full decomposition of supersaturated (Co) solid solution proceeds. In addition, the high-temperature fcc α-Co transformed into low-temperature hcp ε-Co. The respective $T_{eff} = 400$ °C for the Co–Cu system [8].

3. Effective temperature in Cu–Co, Cu–Ag, Cu–In and Cu–Sn alloys

In Cu-rich Co–Cu alloys the situation is even more interesting [28]. The Cu–4.9 wt % Co alloy has been subjected to high pressure torsion in two different states, namely with Co fully dissolved in the Cu-rich matrix (after annealing at 1060 °C for 10 h, Sample 2) and fully precipitated from the Cu matrix (after annealing at 570 °C for 840 h, Sample 1). With an increasing number of rotations, the lattice parameter of Sample 1 decreased and that of Sample 2 increased. After 5 anvil rotations the lattice parameter in both samples becomes almost undistinguishable and corresponds to the solid solution of Co in Cu with 2.5 wt%. In other words, the composition of the solid solution in the Cu – 4.9 wt % Co alloy after the given HPT processing does not depend on the initial state prior to HPT. The composition of Cu-rich matrix in both alloys before and after HPT is shown in the Cu–Co phase diagram (Fig. 1). The solid solution in samples 1 and 2 after HPT contains as much Co, as if they would be annealed at $T_{eff1} = 920 \pm 30$ °C and $T_{eff2} = 870 \pm 30$ °C, respectively.

Thus, the steady-state with respect to the grain size, size of Co precipitates and concentration of Co in a solid solution during HPT is indeed *equifinal* i.e. independent on the starting state. This term was introduced by von Bertalanffi in order to underline the analogy between *equilibrium* for closed systems and *equifinality* for open ones [36]. Such an equifinality has been observed also in similar experiments with Cu–8 wt. % Ag alloy [37]. The effective temperature is $T_{eff} = 780 \pm 1$ °C in this case.

Six Cu–In alloys with 2.3, 4, 5.8, 7, 9.5 and 13.5 at.% In have been studied in Ref. [38]. The Cu–In alloys possess the negative mixing enthalpy. The torsion torque during HPT reached a steady-state after 1–2 anvil rotations. Differently to the alloys with positive mixing enthalpy, the Cu(In) solid solution in the samples 2.3, 4, 5.8, 7, and 9.5 at.% In with did not decompose. However, the precipitates of δ-phase in the Cu–13.5 at. % In alloy partially dissolved and additionally enriched the Cu(In) solid solution. As a result, the concentration of indium in the Cu-matrix becomes at least as high as a sample annealed at $T_{eff} = 574$ °C.

It has been also revealed that high pressure torsion induces phase transformations of certain Hume-Rothery phases (electron

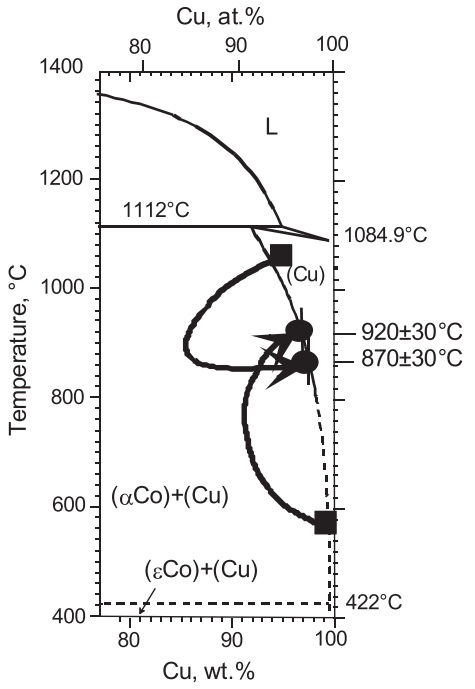

Fig. 1. The Cu-rich part of the Co–Cu phase diagram [35]. The composition of Cu-rich matrix in both alloys before (squares) and after (circles) HPT is shown. Reproduced from Ref. [28] with permission from Elsevier.

compounds) to others [39]. High pressure torsion induces the $\zeta \rightarrow \delta + \varepsilon$ reaction in copper–tin alloys with the appearance of the $\delta + \varepsilon$ phase mixture as after long term annealing in the temperature range $T_{eff} = 350–589$ °C.

Two Cu–Al–Ni shape memory alloys (Cu–13.1 wt% Al–3.8 wt% Ni and Cu–14.4 wt% Al–4.3 wt% Ni) were studied in Ref. [40]. The as-cast alloys were annealed in the one-phase β-area of the Cu–Al–Ni phase diagram (so-called austenite area) and water quenched. As a result, one alloy was in martensitic state (mainly β'_3 with a small amount of γ'_3 phase), and a second one was austenitic (β_3 phase). After HPT, both alloys became ultra-fine grained and contained mainly β'_3 martensite with a certain amount of γ'_3 martensite. This is because HPT drives the precipitation of α_1-phase in Al-poor alloy and the precipitation of γ_1-phase in the Al-rich alloy. This precipitation was followed by the characteristic martensitic transformation. We will not focus here on the details of martensitic transformations in these shape memory alloys. For this review it is important that the HPT-driven precipitation in both Cu–Al–Ni alloys is such as if they were annealed at $T_{eff} = 620 \pm 20$ °C.

4. Effective temperature in Cu–Hf and Cu–Cr alloys

The Cu– 0.7 wt % Cr and Cu– 0.9 wt % Hf alloys have been prepared from high-purity 5 N Cu, Hf and Cr by vacuum induction melting into cylindrical ingots. For HPT processing, the 0.6 mm thick discs were cut from the as-cast ingots, then ground and chemically etched. They were sealed into evacuated silica ampoules with a residual pressure of approximately 4×10^{-4} Pa at room temperature. Cu– 0.7 wt % Cr samples were annealed at 1000 °C for 384 h and at 1040 °C for 478 h, and then quenched in water. Cu–0.9 wt % Hf samples were annealed at 500 °C for 840 h, 550 °C for 2300 h and 900 °C for 384 h, and then quenched in water. The accuracy of the annealing temperature was ±1 °C. The annealed samples were subjected to HPT at room temperature under a pressure of 5 GPa in a Bridgman anvil-type unit (5 rotations of the anvil with the rate of 1 rpm). Samples for microstructural and X-rays investigations were cut from the HPT-processed discs at a distance of 3 mm from the sample center. The transmission electron microscopy (TEM) was performed by TECNAI G2 FEG super TWIN (200 kV) microscope equipped with an energy dispersive X-ray (EDX) spectrometer manufactured by EDAX. TEM foils were prepared by the focused ion beam (FIB) technique. Scanning electron microscopy (SEM) investigations were carried out on a Philips XL30 scanning microscope equipped with a LINK ISIS energy-dispersive X-ray spectrometer from Oxford Instruments. X-ray diffraction (XRD) data were obtained on a Pan Analytical X'Pert (Philips) diffractometer (Cu Kα radiation). Lattice parameter values were estimated using powder diffraction tool of "Fityk software" [41].

The as cast Cu– 0.7 wt % Cr alloy contained elongated primary grains of Cu-based solid solution (with size about 50 × 200 μm) and fine lamellar Cu/Cr eutectic in the (Cu)/(Cu) grain boundaries (GBs). After a long anneal at 1000 °C for 384 h, the Cu– 0.7 wt % Cr alloy contained large grains of Cu-based solid solution (with grain size of 100–200 μm) and few equiaxial large Cr particles with size about 3–10 μm. Cu grains also contain a lot of very fine Cr precipitates with size of 5–10 nm. The Cu– 0.9 wt % Hf alloy after long anneal at 550 °C for 2300 h has large equiaxial grains of (Cu) solid solution with size of about 400 μm and numerous Cu_6Hf particles. The Cu_6Hf particles in the bulk are almost equiaxial with size of 1–5 μm and not faceted. The Cu_6Hf particles in (Cu)/(Cu) grain boundaries are elongated and sometimes form the continuous layers with thickness of 1–3 μm. This indicates complete wetting of (Cu)/(Cu) GBs by solid intermetallic Cu_6Hf like in Zn–Al, Al–Mg and Co–Cu systems [42–44]. The Cu– 0.9 wt % Hf alloy after long anneal at 900 °C for 384 h has large equiaxial grains of (Cu) solid solution with size of about 300–700 μm and few large (3–5 μm) faceted Cu_6Hf particles and some annealing twins are visible. The shape of these twins is different compared to annealing twins in pure copper [45,46]. In particular, they do not contain the so-called 9R facet but the higher-indexed facets in the Σ3 coincidence-sites lattice. Cu matrix also contains numerous very tiny (2–3 nm) Cu_6Hf precipitates.

The HPT deformation leads to the strong grain refinement and full dissolution of Cr precipitates in the Cu–0.7 wt % Cr alloy annealed at 1000 °C [47]. The size of (Cu) grains was about 350 nm [47]. In Cu– 0.9 wt % Hf alloy the HPT deformation also leads to the strong grain refinement, the grain size decreases down to about 200–500 nm and precipitates dissolve.

Fig. 2a shows the dependence of lattice parameter in Cu–0.9 wt % Hf alloy on the temperature obtained by XRD. Open circle marks the lattice parameter of pure copper. Filled squares mark the lattice parameter of samples annealed 500 °C for 840 h, 550 °C for 2300 h and 900 °C for 384 h, and then quenched in water. Open squares mark the lattice parameter of the same samples after additional HPT. The lattice parameter of (Cu) solid solution decreases with increasing Hf content. Before HPT, the lattice parameter of (Cu) solid solution after anneals at 500 and 550 °C is close to that of pure copper because all hafnium is in the Cu_6Hf precipitates (see phase diagram in Fig. 2b). In sample annealed at 900 °C almost more hafnium is solved in (Cu) solid solution and only few large and small Cu_6Hf precipitates can be seen. HPT leads to the grain refinement and dissolution of Cu_6Hf precipitates. The microstructure of samples after HPT is very similar. The lattice parameter is also almost similar in all three samples (Fig. 2a). It means that it is equifinal, as observed in Cu–Co [28] and Cu–Ag [37] alloys. Moreover, it is higher than that in the samples annealed at 900 °C. It means that the effective temperature is $T_{eff} = 970 \pm 40$ °C. In Cu–Cr alloys the lattice parameter increases with increasing concentration of chromium. The lattice parameter of Cu– 0.7 wt % Cr alloy is

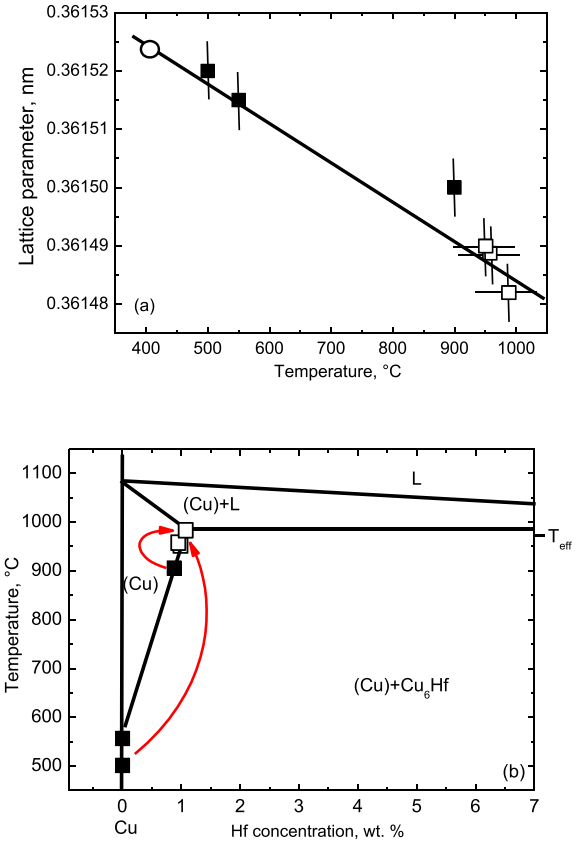

Fig. 2. (a) Dependence of lattice parameter in Cu–0.9 wt % Hf alloy on the temperature obtained by XRD. Open circle marks the lattice parameter of pure copper. Filled squares mark the lattice parameter of samples annealed 500 °C for 840 h, 550 °C for 2300 h and 900 °C for 384 h, and then quenched in water. Open squares mark the lattice parameter of the same samples after additional HPT. (b) Cu-rich side of Cu–Hf phase diagram [35]. Full squares show the composition of (Cu) solid solutions after annealing at 500, 550 and 1000 °C. Open squares show the composition of (Cu) solid solutions after HPT. T_{eff} = 970 ± 40 °C.

0.36164 nm after annealing at 1000 °C for 384 h and 0.36172 nm after annealing at 1040 °C for 478 h. After HPT the lattice parameter of first sample increases up to 0.36172 nm and becomes equal to that of the sample annealed at 1040 °C for 478 h. It means that the fine (Cr) precipitates present in the sample after annealing at 1000 °C completely diluted in (Cu) solid solution [47]. The effective temperature for Cu–Cr alloys, therefore, can be estimated as T_{eff} = 1040 ± 20 °C.

5. Correlation between T_{eff}, activation enthalpy of diffusion and melting temperature

In Ref. [37] a model was developed to describe the competition between dissolution and precipitation during HPT in Cu–Ag alloys. This model describes the dynamic equilibrium between dissolution and precipitation in HPT. It assumes that HPT fixes the composition at matrix-precipitate interfaces. The model shows that HPT-enhanced diffusive mass-transfer is the process controlling the observed steady-state composition in the matrix and precipitate average diameter. Using only the value of bulk diffusion coefficient D one can calculate the steady-state concentration c_m. Consequently, the usage of Cu–Ag phase diagram allows finding the temperature T_{eff} where the c_m is equal to the solubility of Ag in Cu. T_{eff} in Cu–Ag alloys (as well in other Cu-based alloy listed above) is higher than the HPT temperature T_{HPT} (which is close in our experiments at room temperature). Physically, the feature that T_{eff} is always higher than T_{HPT} reflects the fact that the steady-state concentration of vacancies during HPT process is increased in comparison with equilibrium one at T_{HPT} and can be close to that at T_{eff} [48–50].

If we substitute silver in Cu-based solid solution, the diffusion coefficient D would change as well. The higher diffusivity would require the lower T_{eff} and visa versa. Therefore, one can expect the correlation between activation enthalpy of diffusion H_D and effective temperature T_{eff}. Fig. 3a contains the plot showing the correlation between T_{eff} and H_D. The values of H_D were taken from the diffusion handbook [51]. The obvious linear correlation between T_{eff} and H_D can be seen. The increase of H_D leads to the increase of T_{eff}. Physically, such correlation is easy to understand because the increase of H_D means the increase of energy barrier for the diffusion jumps of alloying atoms in copper lattice. Increased energy barrier for diffusion jumps leads to decreased diffusivity and relaxation rate in the dynamic equilibrium during HPT. In turn, slow relaxation, increases the steady-state concentration of non-equilibrium lattice defects (vacancies). As a result, T_{eff} also increases.

However, the second plot in Fig. 3 is less obvious. Fig. 3b shows the correlation between effective temperature T_{eff} and melting temperature T_m of alloying element in various Cu-based alloys. Similar to Fig. 3a, T_{eff} monotonically increases with increasing T_m of alloying element. Such a correlation would be expected if we would

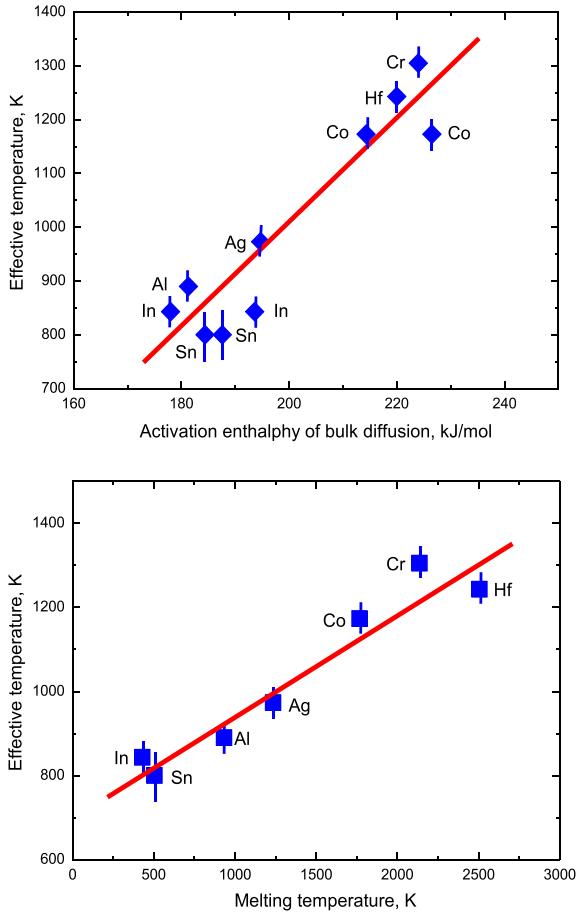

Fig. 3. (a) Dependence between effective temperature of HPT treatment T_{eff} of copper-based solid solutions and activation enthalpy of bulk tracer diffusion H_D of alloying element. (b) Correlation between effective temperature T_{eff} and melting temperature T_m of alloying element in various Cu-based alloys. The values of H_D and T_m were taken from the handbook [51].

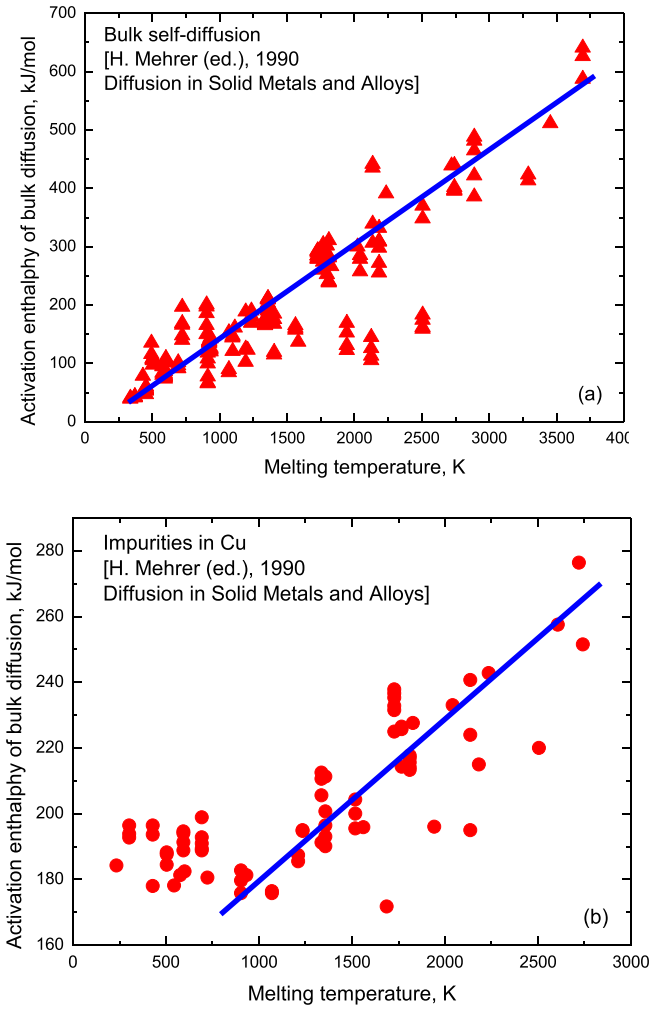

Fig. 4. (a) Dependence between activation enthalpy of bulk self-diffusion H_{DS} and melting temperature T_m. (b) Dependence between activation enthalpy of bulk tracer diffusion H_D in copper-based solid solutions and melting temperature T_m of diffusing alloying component. Data for the plots are taken from Ref. [51].

speak about melting temperature of matrix. The plot in Fig. 4a shows the famous correlation between activation enthalpy of tracer self-diffusion H_{DS} and melting temperature T_m for different pure elements. In Fig. 4a, $H_{DS} = 170\ T_m$. We plotted this correlation using the data from diffusion handbook [51], but the correlation $H_{DS} \sim T_m$ is known since at least 60 years and mentioned in all textbooks on diffusion [[52] and references therein]. In order to explain the correlation between T_{eff} and T_m shown in Fig. 3b and using the data from the same diffusion handbook [51], we plotted the dependence between activation enthalpy of bulk tracer diffusion H_D in copper-based solid solutions and melting temperature T_m of diffusing alloying component (Fig. 4b). A good correlation between H_D and T_m can be observed. H_D monotonously and nearly linearly increases with increasing T_m for $T_m > 1000$ K. We have to underline again here, the T_m in Fig. 4b is NOT the melting temperature of matrix (it is almost the same in our experiments and very close to T_m of copper). T_m in Fig. 4b is the melting temperature of diffusing alloying component. The slope of the straight lien in Fig. 4b is $H_{DS} = 50\ T_m$ and, therefore, about three time less than that in Fig. 4a ($H_{DS} = 170\ T_m$). It means the T_m value for solute elements influences H_D much weaker than the melting temperature of the matrix.

To the best of our knowledge, the correlation between H_D and melting temperature of tracer T_m has been found for the first time. It is strange that previously nobody found it, because the diffusion data for such plot are available since many dozens of years. One possible explanation is that such a correlation (opposite to that shown in Fig. 4a) has no obvious physical explanation. At the moment, we found the linear correlation between H_D and melting temperature of tracer T_m also for gold, silver and some other elements where enough data for tracer H_D are available.

The empirical dependence between T_{eff} and melting temperature T_m of alloying component in copper (Fig. 3b) allows one to predict the behaviour of any Cu-based binary alloy during HPT. For this purpose one needs to know the T_m value of alloying component B. Knowing T_m, one finds the T_{eff} value for B from the $T_{eff} - T_m$ plot (Fig. 3b). Knowing T_{eff}, one can find the solubility $c_B(T_{eff})$ of B at T_{eff} from the Cu–B phase diagram. The $c_B(T_{eff})$ value would be the steady state concentration which has to be attained during HPT. In other words, if the Cu–B would be annealed at $T > T_{eff}$ and quenched, the resulted Cu(B) solid solution would decompose during HPT, fine precipitates of B or Cu-B intermetallic compounds would form in the alloy and concentration of B atoms in Cu would decrease during HPT down to $c_B(T_{eff})$ value. Visa versa, if the Cu–B would be annealed at $T < T_{eff}$, the particles of second phase (B or Cu-B intermetallic compounds) would dilute in the Cu matrix, and concentration of B atoms would increase during HPT up to $c_B(T_{eff})$ value.

The $T_{eff} - T_m$ plot in Fig. 3b is constructed for the HPT at room temperature (RT = 300 K). If the HPT temperature is below RT, the value of D_b in Eq. (1) would decrease. On the other hand, the mechanism of HPT-driven mass transfer (described by the value of D_{ball}) remains more or less the same. It means that below RT the value of $\Delta = D_{ball}/D_b$ would decrease and resulting T_{eff} increases. In other words, the T_{eff} (T_m) lines for $T > 300$ K should be above the line shown in Fig. 3b. Visa versa, above RT the value of $\Delta = D_{ball}/D_b$ would increase and resulting T_{eff} decreases, and T_{eff} (T_m) lines for $T < 300$ K should be above the line shown in Fig. 3b.

We discussed, what happens if the relaxation rate (controlled by D_b) changes and the rate of defects production (described by D_{ball}) remains the same. Can we fix D_b and change D_{ball}? It is possible if we study the action of other SPD modes on precipitation/dissolution process in Cu-based alloy. How can we estimate the D_{ball} of other SPD modes in comparison with that of HPT before direct measurements? The good possibility for rough D_{ball} estimation give the data on steady-state grain size d_{ss} in pure copper which can be obtained in various SPD modes. We can suppose that if the action of other SPD mode is stronger than that of HPT and the rate of defect production is higher, than grain size would be smaller d_{ss} (SPD) < d_{ss} (HPT) and D_{ball} (SPD) > D_{ball} (HPT). Fig. 5 gives such a comparison. It is good visible that HPT allows obtaining the lowest copper grain size in comparison with other SPD modes. Only ball milling (BM) produces smaller grains in copper. It means that D_{ball} of other SPD modes (except of that of BM) is lower in comparison with D_{ball} of HPT. In other words the T_{eff} (T_m) lines for other SPD modes should lie below the line shown in Fig. 3b, and only the values of for T_{eff} ball milling should be higher.

The steady-state grain size d_{ss} as a measure of D_{ball} also permits to predict the values of T_{eff} for other metals (in comparison with those for copper). Thus, the value of d_{ss} increases with increasing stacking fault energy (SFE) [62–64]. One can expect that the values of T_{eff} should be lower in comparison with those for copper. Indeed, for Cu–Zn alloys the plot in Fig. 3b predicts $T_{eff} \approx 850$ K. Aluminium has higher SFE (166 mJ/m^2) in comparison with copper (45 mJ/m^2), and respectively, higher d_{ss} after ECAP (1400 nm for Al and 300 nm for Cu at 0.32 T_m [62]). Therefore, one can expect that for Al–Zn alloys would be lower than that for Cu–Zn alloys ($T_{eff} \approx 850$ K, Fig. 3b). Indeed, the HPT of Al–Zn alloys gives T_{eff} close to 300 K [6,30,65]. Therefore, these examples show that T_{eff} (T_m) plot

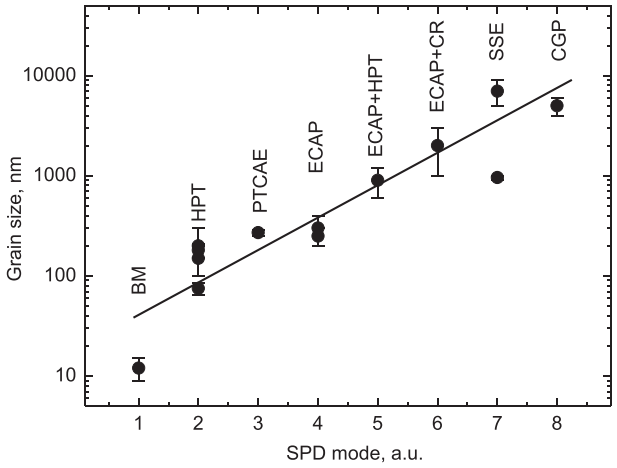

Fig. 5. Steady-state grain size in copper subjected to the different SPD modes: 1 – Ball milling (BM) [53], 2 – High pressure torsion (HPT) [7,28,30,54,55], 3 – Planar twist channel angular extrusion (PTCAE) [56], 4 – Equal channel angular pressing (ECAP) [54,57], 5 – ECAP + HPT [54], 6 – Equal channel angular pressing with following cold rolling (ECAP + CR) [58], 7 – Simple shear extrusion (SSE) [59,60], 8 – Constrained groove pressing (CGP) [61].

(Fig. 3b) obtained in this work for HPT of copper alloys together with comparative plot in Fig. 5 for various SPD methods possess a high predictive power for the behaviour of solid solutions and precipitates under SPD.

6. Conclusions

Severe plastic deformation not only leads to grain refinement but also accelerates mass-transfer and drives phase transformations in the materials. The results of such SPD-driven transitions cannot be explained by the bulk or even grain boundary diffusion at the SPD temperature (which is usually close to room temperature). We analyzed in this review the decomposition of (supersaturated) solid solution and dissolution of precipitates during high pressure torsion in diluted Cu-based Cu–X alloys. The precipitation of particles of a second phase from a solid solution and their dissolution take place simultaneously and compete with each other. During HPT, a certain steady-state concentration C_s of a second component in a solid solution is reached. The solid solution with concentration C_s can be found in a solvus line of a Cu–X phase diagram at a certain effective temperature T_{eff}. It is as if the Cu–X alloy has been annealed at T_{eff}.

The SPD drives mass transfer and forces the atoms to overcome a certain energy barrier. This energy barrier is similar to that for the bulk diffusion. The measure for this barrier is the activation enthalpy of bulk diffusion H_D. We found that T_{eff} linearly increases with increase of activation enthalpy of bulk tracer diffusion H_D. The correlation between activation enthalpy of bulk tracer diffusion H_D and melting temperature T_m of diffusing alloying component has been found for the first time. As a result, T_{eff} linearly increases also with increase of melting temperature T_m of diffusing alloying component. The observed correlations allow one for the first time to predict the behaviour and phase transitions in the Cu-based alloys under high pressure torsion.

The observed correlations allow one to predict the behaviour and phase transitions in the Cu-based alloys under high pressure torsion. If one has a Cu–X alloy and knows the melting temperature of a component X, one can also estimate the respective value of T_{eff}. Knowing the Cu–X phase diagram and T_{eff}, one can estimate the concentration C_s at T_{eff}. If a Cu–X alloy contains precipitates and the (Cu) solid solution with $C < C_s$, then HPT would lead to the increase of C up to C_s and dissolution of precipitates. If a Cu–X alloy contains the (Cu) solid solution with $C > C_s$, then HPT would lead to the decrease of C down to C_s and formation of fine precipitates.

Acknowledgements

The work was supported by the National Science Centre of Poland (grant OPUS 2014/13/B/ST8/04247), the Russian Federal Ministry for Education and Science (Increase Competitiveness Program of NUST«MISiS» implemented by a governmental decree No 211 of 16.03.2013), by the Russian Foundation for Basic Research (grants 14-48-03598 and 16-53-12007), and by Deutsche Forschungsgemeinschaft. The part of research has been performed within the Accredited Testing Laboratories with certificate No. AB 120 issued by the Polish Center of Accreditation according to European standard PN-ISO/IEC 17025:2005 and EA-2/15.

References

[1] R.Z. Valiev, R.K. Islamgaliev, I.V. Alexandrov, Bulk nanostructured materials from severe plastic deformation, Prog. Mater. Sci. 45 (2000) 103–189.
[2] A.M. Glezer, R.V. Sundeev, General view of severe plastic deformation in solid state, Mater. Lett. 139 (2015) 455–457.
[3] X. Sauvage, A. Chbihi, X. Quelennec, Severe plastic deformation and phase transformations, J. Phys. 240 (2010) 012003.
[4] W. Lojkowski, M. Djahanbakhsh, G. Burkle, S. Gierlotka, W. Zielinski, H.J. Fecht, Nanostructure formation on the surface of railway tracks, Mater. Sci. Eng. A 303 (2001) 197–208.
[5] X. Sauvage, X. Quelennec, J.J. Malandain, P. Pareige, Nanostructure of a cold drawn tempered martensitic steel, Scr. Mater. 54 (2006) 1099–1103.
[6] B.B. Straumal, B. Baretzky, A.A. Mazilkin, F. Phillipp, O.A. Kogtenkova, M.N. Volkov, R.Z. Valiev, Formation of nanograined structure and decomposition of supersaturated solid solution during high pressure torsion of Al–Zn and Al–Mg, Acta Mater. 52 (2004) 4469–4478.
[7] A.A. Mazilkin, B.B. Straumal, E. Rabkin, B. Baretzky, S. Enders, S.G. Protasova, O.A. Kogtenkova, R.Z.Valiev, Softening of nanostructured Al–Zn and Al–Mg alloys after severe plastic deformation, Acta Mater. 54 (2006) 3933–3939.
[8] B.B. Straumal, S.G. Protasova, A.A. Mazilkin, E. Rabkin, D. Goll, G. Schütz, B. Baretzky, R.Z. Valiev, Deformation-driven formation of equilibrium phases in the Cu–Ni alloys, J. Mater. Sci. 47 (2012) 360–367.
[9] C.M. Cepeda-Jiménez, J.M. García-Infanta, A.P. Zhilyaev, O.A. Ruano, F. Carreño, Influence of the thermal treatment on the deformation-induced precipitation of a hypoeutectic Al–7 wt% Si casting alloy deformed by high-pressure torsion, J. Alloys Comp. 509 (2011) 636–643.
[10] Y. Ivanisenko, I. MacLaren, X. Sauvage, R.Z. Valiev, H.-J. Fecht, Shear-induced α → γ transformation in nanoscale Fe–C composite, Acta Mater. 54 (2006) 1659–1669.
[11] B.B. Straumal, A.A. Mazilkin, S.G. Protasova, S.V. Dobatkin, A.O. Rodin, B. Baretzky, D. Goll, G. Schütz, Fe–C nanograined alloys obtained by high pressure torsion: structure and magnetic properties, Mater. Sci. Eng. A 503 (2009) 185–189.
[12] V.V. Sagaradze, V.A. Shabashov, Deformation-induced anomalous phase transformations in nanocrystalline FCC Fe–Ni based alloys, Nanostruct. Mater. 9 (1997) 681–684.
[13] B.B. Straumal, S.V. Dobatkin, A.O. Rodin, S.G. Protasova, A.A. Mazilkin, D. Goll, B. Baretzky, Structure and properties of nanograined Fe–C alloys after severe plastic deformation, Adv. Eng. Mater. 13 (2011) 463–469.
[14] A.V. Korznikov, G. Tram, O. Dimitrov, G.F. Korznikova, S.R. Idrisova, Z. Pakiela, The mechanism of nanocrystalline structure formation in Ni_3Al during severe plastic deformation, Acta Mater. 49 (2001) 663–671.
[15] C. Rentenberger, H.P. Karnthaler, Extensive disordering in long-range-ordered Cu_3Au induced by severe plastic deformation studied by transmission electron microscopy, Acta Mater. 56 (2008) 2526–2530.
[16] S.D. Prokoshkin, I.Yu. Khmelevskaya, S.V. Dobatkin, I.B. Trubitsyna, E.V. Tatyanin, V.V. Stolyarov, E.A. Prokofiev, Alloy composition, deformation temperature, pressure and post-deformation annealing effects in severely deformed Ti–Ni based shape memory alloys, Acta Mater. 53 (2005) 2703–2714.
[17] A.A. Mazilkin, G.E. Abrosimova, S.G. Protasova, B.B. Straumal, G. Schütz, S.V. Dobatkin, A.S. Bakai, Transmission electron microscopy investigation of boundaries between amorphous "grains" in $Ni_{50}Nb_{20}Y_{30}$ alloy, J. Mater. Sci. 46 (2011) 4336–4342.
[18] V.V. Stolyarov, D.V. Gunderov, A.G. Popov, V.S. Gaviko, A.S. Ermolenko, Structure evolution and changes in magnetic properties of severe plastic deformed Nd(Pr)–Fe–B alloys during annealing, J. Alloys Comp. 281 (1998) 69–71.
[19] B.B. Straumal, A.A. Mazilkin, S.G. Protasova, D.V. Gunderov, G.A. López, B. Baretzky, Amorphization of crystalline phases in the Nd-Fe-B alloy driven

by the high-pressure torsion, Mater. Lett. 161 (2015) 735–739.
[20] Y. Ivanisenko, I. MacLaren, X. Sauvage, R.Z. Valiev, H.J. Fecht, Shear-induced α → γ transformation in nanoscale Fe–C composite, Acta Mater. 54 (2006) 1659–1669.
[21] M.T. Pérez-Prado, A.P. Zhilyaev, First experimental observation of shear induced hcp to bcc transformation in pure Zr, Phys. Rev. Lett. 102 (2009) 175504.
[22] K. Edalati, Z. Horita, Y. Mine, High-pressure torsion of hafniurn, Mater. Sci. Eng. A 527 (2010) 2136–2141.
[23] B.B. Straumal, A.R. Kilmametov, Yu. Ivanisenko, A.S. Gornakova, A.A. Mazilkin, M.J. Kriegel, O.B. Fabrichnaya, B. Baretzky, H. Hahn, Phase transformations in Ti-Fe alloys induced by high pressure torsion, Adv. Eng. Mater. 17 (2015) 1835–1841.
[24] A.M. Glezer, M.R. Plotnikova, A.V. Shalimova, S.V. Dobatkin, Severe plastic deformation of amorphous alloys: I. Structure and mechanical properties, Bull. Russ. Ac. Sci. Phys. 73 (2009) 1233–1236.
[25] S. Hóbor, Á. Révész, A.P. Zhilyaev, Zs. Kovácz, Different nanocrystallization sequence during high pressure torsion and thermal treatments of amorphous $Cu_{60}Zr_{20}Ti_{20}$ alloy, Rev. Adv. Mater. Sci. 18 (2008) 590–592.
[26] G.E. Abrosimova, A.S. Aronin, S.V. Dobatkin, S.D. Kaloshkin, D.V. Matveev, O.G. Rybchenko, E.V. Tatyanin, I.I. Zverkova, The formation of nanocrystalline structure in amorphous Fe-Si-B alloy by severe plastic deformation, J. Metastab. Nanocryst. Mater 24 (2005) 69–72.
[27] Zs. Kovács, P. Henits, A.P. Zhilyaev, N.Q. Chinh, Á. Révész, Microstructural characterization of the crystallization sequence of a severe plastically deformed Al-Ce-Ni-Co amorphous alloy, Mater. Sci. Forum 519–521 (2006) 1329–1334.
[28] B.B. Straumal, A.R. Kilmametov, Yu.O. Kucheev, L. Kurmanaeva, Yu. Ivanisenko, B. Baretzky, A. Korneva, P. Zięba, D.A. Molodov, Phase transitions during high pressure torsion of Cu–Co alloys, Mater. Lett. 118 (2014) 111–114.
[29] G. Martin, Phase stability under irradiation: ballistic effects, Phys. Rev. B 30 (1984) 1424–1436.
[30] B.B. Straumal, A.A. Mazilkin, B. Baretzky, E. Rabkin, R.Z. Valiev, Accelerated diffusion and phase transformations in Co–Cu alloys driven by the severe plastic deformation, Mater. Trans. 53 (2012) 63–71.
[31] B.B. Straumal, L.M. Klinger, L.S. Shvindlerman, The influence of pressure on indium diffusion along single tin–germanium interphase boundaries, Scr. Metall. 17 (1983) 275–279.
[32] D.A. Molodov, B.B. Straumal, L.S. Shvindlerman, The effect of pressure on migration of the [001] tilt grain boundaries in the tin bicrystals, Scr. Metal. 18 (1984) 207–211.
[33] G. Thomas, H. Mori, H. Fujita, Electron irradiation induced crystalline amorphous transitions in Ni–Ti alloys, Scr. Metall. 16 (1982) 589–592.
[34] A.A. Mazilkin, B.B. Straumal, M.V. Borodachenkova, R.Z. Valiev, O.A. Kogtenkova, B. Baretzky, Gradual softening of Al–Zn alloys during high pressure torsion, Mater. Lett. 84 (2012) 63–65.
[35] T.B. Massalski (Ed.), Binary Alloy Phase Diagrams, second ed., ASM International, Materials Park, OH, 1990.
[36] L. von Bertalanffy, General system theory: a new approach to unity of science, Hum. Biol. 23 (1951) 302–312.
[37] B.B. Straumal, V. Pontikis, A.R. Kilmametov, A.A. Mazilkin, S.V. Dobatkin, B. Baretzky, Competition between precipitation and dissolution in Cu–Ag alloys under high pressure torsion, Acta Mater. 122 (2017) 60–71.
[38] B.B. Straumal, A.R. Kilmametov, A.A. Mazilkin, L. Kurmanaeva, Y. Ivanisenko, A. Korneva, P. Zięba, B. Baretzky, Transformations of Cu(In) supersaturated solid solutions under high-pressure torsion, Mater. Lett. 138 (2015) 255–258.
[39] B.B. Straumal, A.R. Kilmametov, Yu. O. Kucheev, K.I. Kolesnikova, A. Korneva, P. Zięba, B. Baretzky, Transformations of Hume-Rothery phases under the action of high pressure torsion, JETP Lett. 100 (2014) 376–379.
[40] B.B. Straumal, A.R. Kilmametov, G.A. López, I. López-Ferreño, M.L. Nó, J. San Juan, H. Hahn, B. Baretzky, High-pressure torsion driven martensite-austenite transformations in Cu–Al–Ni shape memory alloys, Acta Mater. 122 (2017) in press.
[41] M. Wojdyr, Fityk: a general-purpose peak fitting program, J. Appl. Cryst. 43 (2010) 1126–1128.
[42] G.A. López, E.J. Mittemeijer, B.B. Straumal, Grain boundary wetting by a solid phase; microstructural development in a Zn–5 wt.% Al alloy, Acta Mater. 52 (2004) 4537–4545.
[43] B.B. Straumal, B. Baretzky, O.A. Kogtenkova, A.B. Straumal, A.S. Sidorenko, Wetting of grain boundaries in Al by the solid Al_3Mg_2 phase, J. Mater. Sci. 45 (2010) 2057–2061.
[44] B.B. Straumal, O.A. Kogtenkova, A.B. Straumal, Yu.O. Kuchyeyev, B. Baretzky, Contact angles by the solid-phase grain boundary wetting in the Co–Cu system, J. Mater. Sci. 45 (2010) 4271–4275.
[45] B.B. Straumal, S.A. Polyakov, E.J. Mittemeijer, Temperature influence on the faceting of Σ3 and Σ9 grain boundaries in Cu, Acta Mater. 54 (2006) 167–172.
[46] B.B. Straumal, O.A. Kogtenkova, A.S. Gornakova, V.G. Sursaeva, B. Baretzky, Review: grain boundary faceting-roughening phenomena, J. Mater. Sci. 51 (2016) 382–404.
[47] A. Korneva, B. Straumal, A. Kilmametov, R. Chulist, P. Straumal, P. Zięba, Phase transformations in a Cu-Cr alloy induced by high pressure torsion, Mater. Charact. 114 (2016) 151–156.
[48] B.B. Straumal, O.A. Kogtenkova, R.Z. Valiev, P. Zięba, B. Baretzky, Diffusion and phase transitions accelerated by severe plastic deformation, Diffus. Found. 5 (2015) 95–108.
[49] B. Oberdorfer, E.-M. Steyskal, W. Sprengel, W. Puff, M. Zehetbauer, R. Pippan, R. Wuerschum, In situ probing of fast defect annealing in Cu and Ni with a high-intensity positron beam, Phys. Rev. Lett. 105 (2010) 146101.
[50] J. Čížek, O. Melikhova, Z. Barnovská, I. Procházka, R.K. Islamgaliev, Vacancy clusters in ultra fine grained metals prepared by severe plastic deformation, J. Phys. Conf. Ser. 443 (2013) 012008.
[51] H. Mehrer (Ed.), Diffusion in Solid Metals and Alloys, Landolt-börnstein New Series, Gr III, vol. 26, Springer-Verlag, Berlin, 1990.
[52] H. Mehrer, Diffusion in Solids. Fundamentals, Methods, Materials, Diffusion-controlled Processes, Springer-Verlag, Berlin, Heidelberg, 2007, 650 pp.
[53] M. Azabou, T. Makhlouf, J. Saurin, L. Escoda, J.J. Suñol, M. Khitouni, A study of densification and phase transformations of nanocomposite Cu–Fe prepared by mechanical alloying and consolidation process, Int. J. Adv. Manuf. Technol. 87 (2016) 981–987.
[54] N. Lugo, N. Llorca, J.M. Cabrera, Z. Horita, Microstructures and mechanical properties of pure copper deformed severely by equal-channel angular pressing and high pressure torsion, Mater. Sci. Eng. A 477 (2008) 366–371.
[55] J. Čížek, M. Janeček, O. Srba, R. Kužel, Z. Barnovská, I. Procházka, S. Dobatkin, Evolution of defects in copper deformed by high-pressure torsion, Acta Mater. 59 (2011) 2322–2329.
[56] M. Shamsborhan, M. Ebrahimi, Production of nanostructure copper by planar twist channel angular extrusion process, J. Alloys Comp. 682 (2016) 552–556.
[57] C.L. Tang, H. Li, S.Y. Li, Effect of processing route on grain refinement in pure copper processed by equal channel angular extrusion, Trans. Nonferr. Met. Soc. China 26 (2016) 1736–1744.
[58] Z.N. Mao, R.C. Gu, F. Liu, Y. Liu, X.Z. Liao, J.T. Wang, Effect of equal channel angular pressing on the thermal-annealing-induced microstructure and texture evolution of cold-rolled copper, Mater. Sci. Eng. A 674 (2016) 186–192.
[59] E. Bagherpour, F. Qods, R. Ebrahimi, H. Miyamoto, Microstructure quantification of ultrafine grained pure copper fabricated by simple shear extrusion (SSE) technique, Mater. Sci. Eng. A 674 (2016) 221–231.
[60] E. Bagherpour, F. Qods, R. Ebrahimi, H. Miyamoto, Microstructure evolution of pure copper during a single pass of simple shear extrusion (SSE): role of shear reversal, Mater. Sci. Eng. A 666 (2016) 324–338.
[61] P.C. Yadav, A. Sinhal, S. Sahu, A. Roy, S. Shekhar, Microstructural inhomogeneity in constrained groove pressed Cu-Zn alloy sheet, J. Mater. Eng. Perform. 25 (2016) 2604–2614.
[62] F. Liu, H. Yuan, J. Yin, J.T. Wang, Influence of stacking fault energy and temperature on microstructures and mechanical properties of fcc pure metals processed by equal-channel angular pressing, Mater. Sci. Eng. A 662 (2016) 578–587.
[63] W. Wei, S.L. Wang, K.X. Wei, I.V. Alexandrov, Q.B. Du, J. Hu, Microstructure and tensile properties of Cu–Al alloys processed by ECAP and rolling at cryogenic temperature, J. Alloys Comp. 678 (2016) 506–510.
[64] Y.Z. Cao, X.S. Zhao, W.D. Tu, Y.D. Yan, F.L. Yu, Plastic deformation mechanisms in face-centered cubic materials with low stacking fault energy, Mater. Sci. Eng. A 676 (2016) 241–245.
[65] B. Straumal, A. Korneva, P. Zięba, Phase transitions in metallic alloys driven by the high pressure torsion, Arch. Civ. Mech. Eng. 14 (2014) 242–249.